Scintillators

Mater. Res. Soc. Symp. Proc. Vol. 1341 © 2011 Materials Research Society
DOI: 10.1557/opl.2011.1205

Transparent Lu_2O_3:Eu Ceramics

Zachary M. Seeley, Joshua D. Kuntz, Nerine J. Cherepy, and Stephen A. Payne

Chemical Sciences Division, Lawrence Livermore National Laboratory, Livermore, CA 94550-9698, U.S.A.

ABSTRACT

We are developing highly transparent ceramic oxide scintillators for high energy (MeV) radiography screens. Lutetium oxide doped with europium (Lu_2O_3:Eu) is the material of choice due to its high light yield and stopping power. As an alternative to hot-pressing, we are utilizing vacuum sintering followed by hot isostatic pressing (HIP). Nano-scale starting powder was uniaxially pressed into compacts and then sintered under high vacuum, followed by HIP'ing. Vacuum sintering temperature proved to be a critical parameter in order to obtain highly transparent Lu_2O_3:Eu. Under-sintering resulted in open porosity disabling the driving force for densification during HIP'ing, while over-sintering lead to trapped pores in the Lu_2O_3:Eu grain interiors. Optimal vacuum sintering conditions allowed the pores to remain mobile during the subsequent HIP'ing step which provided enough pressure to close the pores completely resulting in fully-dense highly transparent ceramics. Currently, we have produced 3 mm thick by 4.5 cm diameter ceramics with excellent transparency, and anticipate scaling to larger sizes while maintaining comparable optical properties.

INTRODUCTION

Transparent polycrystalline ceramics have gained significant interest for applications in laser host materials, high index lenses, transparent armor, radiation detectors, and radiography screens [1-5]. They can be formed in a wider range of compositions, sizes, shapes, and at lower cost than single crystals. Transparent ceramics are however limited to cubic crystal structure materials, and optimized processing is necessary to achieve full density and transparency.

Lutetium oxide doped with europium (Lu_2O_3:Eu) has become a material of interest as a scintillating radiography screen due to its high density and x-ray stopping power, efficient conversion to visible light, and visible emission at ~600 nm coupling well with silicon CCDs [6,7]. Due to the high melting point of Lu_2O_3 (~2400°C), sintering to full density is challenging. Conventionally, hot-pressing overcomes this obstacle by applying pressure and temperature simultaneously [8]. However, along with this technique come a highly reducing environment and potential for contamination from the graphite tooling, requiring a post-treatment anneal which often degrades the transparency.

In this work, we have employed the sinter-HIP method to obtain highly transparent Lu_2O_3. Under this process, the ceramic is vacuum sintered to closed porosity and then subsequently HIP'ed under inert argon gas pressure to full density. This method allows consolidation in a less reducing environment and lower potential for contamination.

EXPERIMENT

Lu_2O_3 doped with 5at.% Eu ($Lu_{1.9}Eu_{0.1}O_3$) nanopowder was synthesized via the flame spray pyrolysis (FSP) method by Nanocerox^{TM} (Ann Arbor, MI). As received powder had a specific surface area of 22 m^2/g and was crystallized in the cubic bixbyite structure.

Nanopowder was suspended in an aqueous solution of polyethylene glycol (PEG) and ammonium polymethacrylate using an ultrasonic probe (Cole Parmer, Vernon Hills, Il) and a high shear mixer (Thinky, Japan). This suspension was spray dried (Buchi, New Castle, DE) at 210°C into flowing nitrogen to protect the organics. The dried powder was then sieved (<50μm) to create uniform agglomerates of nanoparticles with an even distribution of organic additives. Formulated nanoparticles were then uniaxially pressed at 50 MPa to form green compacts approximately 35% dense, followed by calcination in air to remove the organics. Calcined compacts were then loaded into a tungsten element vacuum furnace (Thermal Technologies, Santa Rosa, CA) and sintered under a vacuum of $<2\times10^{-6}$ Torr at temperatures ranging between 1575 and 1850°C. The sintered structures were then hot isostatically pressed (HIP'ed) under 200 MPa of inert argon gas pressure at 1850°C for 4 h in a tungsten element HIP (American Isostatic Presses, Columbus, OH). Ceramic surfaces were then ground flat and parallel and given an inspection polish to qualify transparencies. Optical microscopy was used to characterize transparency on a micrometer scale.

RESULTS AND DISCUSSION

The sinter-HIP methodology for densifying powder compacts is a two step process by which the compacts are first vacuum sintered to closed porosity followed by HIP'ing under inert argon gas pressure at high temperatures [9]. During the vacuum sinter step the initial and intermediate stages of sintering are occurring. First necks form between particles. During the intermediate sintering stage, the necks are growing, forming grain boundaries, and pores begin to shrink causing sample densification. With sufficient densification, the pores between the grains are no longer interconnected at which point the compact reaches closed porosity. This step is performed in a high vacuum so that when the pores close to the external surface only vacuum remains trapped in the pores. At this point, external pressure can be applied in the form of an inert gas (argon) at high temperature without the gas infiltrating the porosity of the compact. The pressure provides a secondary driving force for material to diffuse into the vacuum filled pores. In the final stage of sintering the porosity is eliminated and grains begin to grow forming the fully dense ceramic [10].

In the sinter-HIP process, the vacuum sintering temperature is critical to optimize in order to form transparent ceramics. Figure 1 shows photographs of vacuum sintered Lu_2O_3:Eu before and after the HIP'ing step to show the importance of optimizing the vacuum sintering temperature. The sample sintered at 1575°C clearly did not have closed porosity. During the HIP'ing step the argon infiltrated the pores of this sample resulting in very little densification. Samples vacuum sintered between 1600 and 1650°C show high optical transparency after the HIP'ing step, but as the vacuum sintering temperature increased the transparency degrades due to over-sintering. Vacuum sintering at 1600°C was enough to reach closed porosity for the given green density yet it was low enough not to initiate the final stage of sintering. As the vacuum sintering temperature increased up to 1850°C the final stage of sintering begins to occur

accompanied by grain growth. In vacuum sintered samples with larger grain size the grain boundary area decreases allowing fewer pathways for atomic diffusion and pore removal during the HIP'ing step.

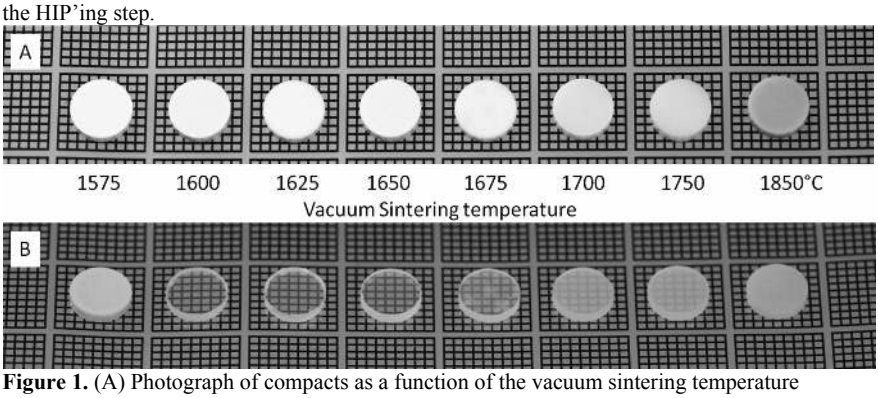

Figure 1. (A) Photograph of compacts as a function of the vacuum sintering temperature between 1575 and 1850°C, and (B) the same compacts after HIP'ing at 1850°C. Samples display a red-orange color luminescence under UV excitation.

To better understand the loss of transparency with increased sintering temperature, samples were characterized optically on the micron scale. Figure 2 shows optical micrographs of HIP'ed samples that were vacuum sintered between 1625 and 1700°C. The focal plane of the optical microscope was focused into the interior of the samples to view the bulk scattering defects, therefore only some of the defects are in focus and others are above and below the focal plane. In the sample vacuum sintered at 1625°C, very few pores are visible and only a slight reflection of light at the grain boundaries can be seen. As the vacuum sintering temperatures increases the number of visible defects increases correspondingly. When the vacuum sintering temperature reaches 1675°C small agglomerations of pores are noticed and by 1700°C the center of each grain is filled with a large pore agglomeration. However, no pores are visible near the grain boundaries. This result indicates that vacuum sintering at higher temperatures resulted in pores becoming entrapped in the interior of each grain. Then, during the subsequent HIP step, residual porosity at the grain boundaries was removed but grain-entrapped pores were not. Vacuum sintering at lower temperatures (i.e. 1625°C) resulted in the ideal microstructure of small grains with pores located on the grain boundaries and easily removed during the HIP'ing step.

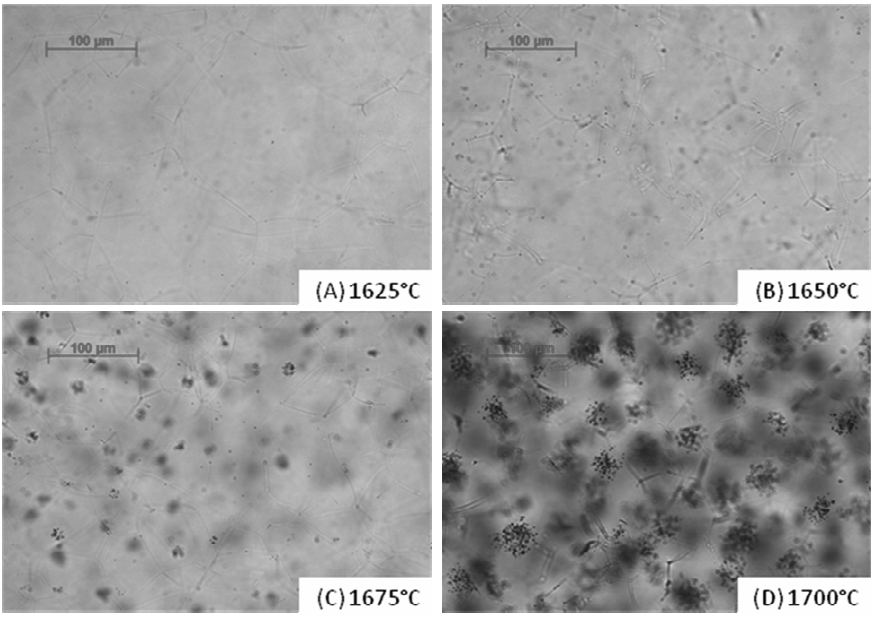

Figure 2. Optical micrographs focused into the interior of the transparent HIP'ed Lu_2O_3:Eu as a function of the vacuum sintering temperature (A) 1625, (B) 1650, (C) 1675, and (D) 1700°C.

The scintillator screen size determines the maximum object size and magnification that can be imaged by X-ray CT. Therefore, we are utilizing this sinter-HIP processing method to scale up to a size useful in industrial radiography screens. Figure 3 shows a 44g part that is ~4.5 cm in diameter and has equivalent transparency to the smaller test coupons. Larger diameter

ceramics are in progress.

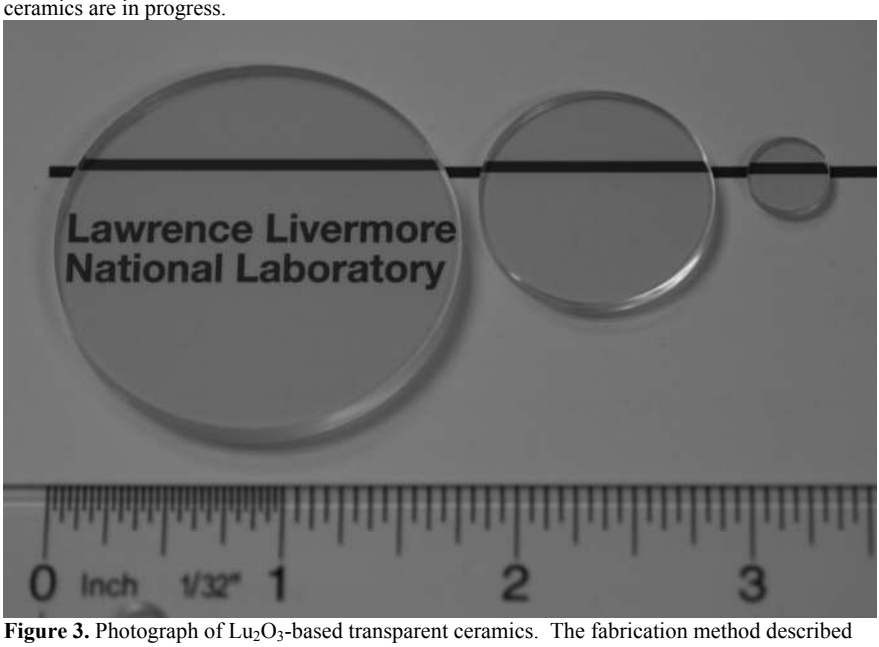

Figure 3. Photograph of Lu_2O_3-based transparent ceramics. The fabrication method described herein allows increased part size while maintaining the high degree of transparency.

CONCLUSIONS

Transparent Lu_2O_3:Eu ceramics were fabricated via the vacuum sinter HIP method. Vacuum sintering temperature proved to be a critical parameter in order to achieve high transparency. Under sintering resulted in open porosity rendering the HIP'ing step ineffective, while over sintering resulted in grain-entrapped porosity with low mobility during the HIP step. The best processing conditions are being used to increase maximum part size for large area scintillator screens.

ACKNOWLEDGMENTS

Thanks to Todd Stefanik of Nanocerox Inc., Jeff Roberts for flame spray synthesis, and Scott Fisher for mechanical fabrication. This work performed under the auspices of the U.S. Department of Energy by Lawrence Livermore National Laboratory under Contract DE-AC52-07NA27344 and funded by the US DOE, Office of NNSA, Enhanced Surveillance Subprogram (Patrick Allen). LLNL-PROC-480414

REFERENCES

1. A. Ikesue, Y. Aung, T. Yoda, S. Nakayama, T. Kamimura, Optical Materials 29, 1289 (2007).
2. U. Peuchert, Y. Okano, Y. Menke, S. Reichel, A. Ikesue, J. European Ceram. Soc. 29, 283 (2009).
3. R. Klement, S. Rolc, R. Mikulikova, J. Krestan, J. European Ceram. Soc. 28, 1091 (2008).
4. N. Cherepy, S. Payne, S. Asztalos, G. Hull, J. Kuntz, T. Niedermayr, S. Pimputkar, J. Roberts, R. Sanner, T. Tillotson, E. Loef, C. Wilson, K. Shah, U. Roy, R. Hawrami, A. Burger, L. Boatner, W. Choong, W. Moses, IEEE Tran. Nuc. Sci., 56, 873 (2009).
5. T. T. Farman, R. H. Vandre, J. C. Pajak, S. R. Miller, A. Lempicki, A. G. Farman, Oral Surg. Oral Med. Oral Pathol. Oral Radiol. Endod. 101, 219 (2006).
6. A. Lempicki, C. Brecher, P. Szupryczynski, H. Lingertat, V. Nagarkar, S. Tipnis, S. Miller, Nuc. Inst. Meth. Phys. Res. A 488, 579 (2002).
7. Y. Shi, Q. W. Chen, J. L. Shi, Optical Materials 31, 729 (2009).
8. D. J. Wisniewski, L. A. Boatner, J. S. Neal, G. E. Jellison, J. O. Ramey, A. North, M. Wisniewska, A. E. Payzant, J. Y. Howe, A. Lempicki, C. Brecher, J. Glodo, IEEE Trans. Nuc. Sci. 55, 1501 (2008).
9. J. Echeberria, J. Tarazona, J. He, T. Butler, F. Castro, J. European Ceram. Soc. 22, 1801 (2002).
10. R. M. German, *Powder Metallurgy Science*, 2nd ed., Metal Powder Industries Federation, Ney Jersey, (1984) p. 261-264.

Mater. Res. Soc. Symp. Proc. Vol. 1341 © 2011 Materials Research Society
DOI: 10.1557/opl.2011.1100

Nuclear Radiation Detection Scintillators based on ZnSe(Te) crystals.

Volodymyr D. Ryzhikov

Institute for Scintillation Materials of STC "Institute for Single Crystals" NAS of Ukraine, 60 Lenin Ave., Kharkov, 61001, Ukraine

ABSTRACT

We describe development of semiconductor scintillators (SCS) on the basis of $A^{II}B^{VI}$ compounds has bridged the gap in a series of "scintillator-photodiode" detectors used in modern multi-channel low-energy devices for visualization of hidden images (tomographs, introscopes). In accordance with the requirements of eventual applications, such SCS materials as ZnSe(Te) show the best matching of intrinsic radiation spectra to photosensitivity spectra of silicon photodiodes (PD) among the materials of similar kind. They are characterized by high radiation and thermal stability of their output parameters, as well as by high conversion efficiency. In this work, a thermodynamic model is described for interaction of isovalent dopants (IVD) with intrinsic point defects of $A^{II}B^{VI}$ semiconductor structures at different ratios of their charges, a decisive role of IVD is shown in formation of the luminescence centers, kinetics of solid-phase reactions and the role of a gas medium are considered under real preparation conditions of ZnSe(Te) scintillation crystals, and luminescence mechanisms in IVD-doped SCS are discussed.

INTRODUCTION

The use of $A^{II}B^{VI}$ compounds, namely, CdS(Te), as highly efficient scintillators was first proposed by J.Thomas e.a. [1,2]. They also assumed that the scintillation mechanism could be determined by radiative recombination centers on isoelectronic traps. Otherwise, in [3] it was shown that luminescence related to isoelectronic traps (IET) is of exciton character, and the corresponding emission spectra, e.g., in ZnTe(O) and $A^{III}B^{V}$ compounds are narrow discrete lines, as distinct from broad diffuse bands characteristic for the centers involving intrinsic defects. The luminescence maximums and the character of the bands are similar to centers involving defects introduced by other means, such as radiation damage [4,5] and thermal treatment [6].

Thus, an isovalent dopant (IVD) atom, differing from the substituted atom by its ion radius and electronegativity, stimulates formation of defects in the neighboring sublattice. In particular, J.Watkins [7] showed by EPR methods that introduction of tellurium into zinc selenide leads to formation of vacancies Zn(V_{Zn}); the displaced Zn moves to the interstitial position, and the V_{Zn} - Zn_i complex, stable up to 400 K, is formed in the vicinity of tellurium atom.

Alongside CdS(Te), other scintillators with IVD are of great interest. We were the first to obtain scintillator ZnSe(Te) [8,9]. As distinct from CdS(Te), its luminescence efficiency is comparable to or higher than in traditional materials like CsI(Tl). At present, ZnSe(Te) scintillators are widely used in inspection equipment.

In a series of studies ([10-12] and others] we have considered in detail thermodynamics of defect formation, preparation methods of ZnSe(Te) and its main characteristics.

These results are briefly summarized in the present work.

EXPERIMENT

Preparation technology of scintillation crystals ZnSe(Te) is based on the known method of crystal growth from the melt [12] using the Bridgman technique in vertical compression, furnaces under inert gas (argon) pressure up to $5 \cdot 10^6$ Pa. Growth rate is 2 – 5 mm/hour, with temperature in the melt zone – up to 1850 K; crystals are grown in graphite crucibles. After growth, crystals are annealed in a vapour of Zn for enhancement and spectral stabilization of luminescence in the 610 – 640 nm region.

To determine optimum technological parameters of the preparation process of ZnSe(Te) , we have studied in detail physical chemistry, thermodynamics and kinetics of interaction of the components in the system ZnSe – ZnTe, by accounting for the composition of the gaseous medium and construction materials of the growth equipment [12-14]. The technology developed by us allows one to obtain reproducibly two types of ZnSe(Te) crystals (mass up to 600 g, diameter up to 40 mm), which are called conventionally “fast” and “slow” scintillators. The main characteristics of there crystals are presented in Tables I.

Table I. Main parameters of scintillation crystals ZnSe(Te).

Parameter	Value
Melting point, K	1773-1793 (depending on [Te])
Density ρ, g/cm^3	5.42
Effective atomic number, Z_{eff}	33
Emission maximum λ_m at 300 K, nm: “fast” scintillator “slow” scintillator	 610 640
Refractive index for λ_m = 610-640 nm	2.58 – 2.61
Attenuation coefficient at λ_m, cm^{-1}	0.05 – 0.15
Decay time, τ, μs: “fast” scintillator “slow” scintillator	 1 – 3 30 – 70
Afterglow, %	< 0.05 after 3 ms
Light yield, photons/MeV γ	$8 \cdot 10^4$
Light output in relation to CsI(Tl), % for X-rays with E<100 keV (CsI(Tl)=100): at 4 mm thickness at 2 mm thickness	 up to 100 up to 170
Matching coefficient between scintsllator and photodiode	up to 0.9

When crystals of $A^{II}B^{VI}$ compounds are grown from the melt under pressure, deviations from stoichiometry in the grown crystals can be larger than 1%. As growth is carried out in semipermeable graphite crucibles, the stoichiometry of the solid crystalline phase is affected by two independent processes — diffusion of the initial charge components through crucible walls and their evaporation.

These processes lead to formation of an ensemble of intrinsic point defects (IPD) of the crystal structure. These defects can be interstitial atoms of metal M_I or chalcogene M_X, vacancies of both types V_M, V_X, anti-structural defects M_X, X_M, complexes of defects involving impurity atoms, with each defect able to exist in several charge states. It is considered that perturbing effects of IPD are localized and extend to several interatomic distances. Formation of vacancies is energetically more favorable in the process of crystallization, but when diffusion processes are predominant, in the case when the melt or crystal are in the atmosphere with excess of one of the components, interstitial IPD are mostly formed, Figure 1.

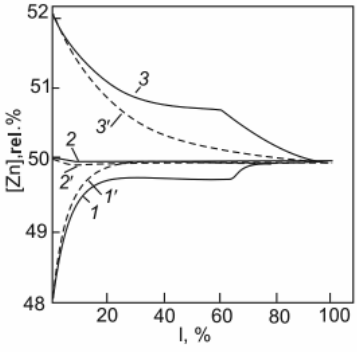

Figure 1. Variation of composition along crystal length in crystals grown by zone melting (1, 2, 3) and directional crystallization (1', 2', 3') at 1800 K and p = 2 MPa, Δz = 1 mm, v = 19.5 μm/s; x_0 = 0.48 (1, 1′), 0.50 (2, 2'), 0.52 (3,3'). [15]

DISCUSSION

Though IVD have the same valence as the substituted lattice atom, such important parameters as ionization energy, electronegativity, ionicity of bonds with atoms of the neighboring sublattice, ion and covalent radii can be substantially different. Bond energy of charge carriers with IVD is by an order of magnitude lower than with donor (D) or acceptor (A) dopants; at the same time, charge localization on IVD is much higher. This combination results in appearance of isolated local states inside the band gap (upon introduction of IVD of the 1st type) with energy levels serving as centers of quenching or emission, or changes in the zone spectrum of allowed bands (IVD of the 2nd type). A criterion for formation of local levels in the band gap is the difference between potential energy values of the IVD atom and the substituted atom [12,16,17]: